Copyright © 2002 Tech Science Press CMES, vol.3, no.3, pp.279-298, 2002

Piecewise Linear Models for Interfaces and Mixed Mode Cohesive Cracks [1]

G. Cocchetti[2], G. Maier[2] and X. P. Shen [3]

Abstract: Interface models mean here relationships between displacement jumps and tractions across a locus of displacement discontinuities. Frictional contact and quasi-brittle fracture interpreted by cohesive crack models are typical mechanical situations concerned by the present unifying approach. Plastic-softening multidissipative interface models are studied in piecewise linear formats, i.e. assuming linearity for yield functions, plastic potentials and relationships between static and kinematic internal variables. The properties and the pros and cons of such simplified models in a variety of formulations (fully non-holonomic in rates, holonomic and in finite steps), all mathematically described as linear complementarity problems, are comparatively investigated in view of overall analyses of structures (like e.g. concrete dams) which include joints and/or are exposed to quasi-brittle fracture processes.

keyword: Interface and joint models, piecewise linearisation, time-integration.

1 Introduction

1.1 Antecedents and motivations

In a number of engineering situations, the computer simulation of nonlinear structural responses to loads involves the definition of a locus (denoted henceforth by Γ) of possible discontinuities of the displacement field. This locus has a lesser dimensionality (by one) with respect to that of the domain of the problem and is characterised by a constitutive model which relates the displacement jump, represented by vector **w**, to the traction, say vector **p**, exchanged across it. Such model will be referred to herein as interface model, briefly IM.

The above general definition of IM concerns a variety of localised, usually dissipative, phenomena and covers idealisations of them frequently adopted for overall analysis and design of engineering structures: unilateral contacts; artificial joints; interfaces prone to debonding in heterogeneous structures (and in laminates and composite materials at the microscale); existing cracks; process zones interpreted by cohesive crack models in quasi-brittle fracture mechanics.

In some categories of structures, specifically in concrete dams which promoted this study, the afore-listed kinds of interfaces may occur simultaneously and, hence, make a unifying frame desirable. The above localised phenomena frequently represent the main source of nonlinearity and dissipation; therefore they lead to structural analysis procedures which assume elastic material behaviour everywhere outside Γ_d and, in kinematically linear ("small deformation") regimes, confine all nonlinearities on Γ_d.

In the above specified broad sense, several IMs have been proposed in the literature, with a diversity of basic features and contexts, see e.g. Abraham (2000), Ahmadi, Izadinia and Bachmann (2001), Carol, Prat and Lopez (1997), Corigliano (1993), Fakharian and Evgin (2000), Hassanzadeh (1990), Lotfi and Shing (1994), Mroz and Giambanco (1996), Xu and Needleman (1994), Wei, Chow and Liu (2000). In the variety of properties exhibited by available IMs the following ones are worth mentioning: an elastic phase, sometimes susceptible to damage in the sense of stiffness deterioration; alternatively rigid-inelastic behaviour; perfect plasticity (like in traditional Coulomb friction models) or softening, which is essential ingredient of fracture process simulations in concrete-like solids; associative flow rules or non-associativity as a manifestation of internal friction; history-dependent (non-holonomic) models, realistically reflecting irreversible energy dissipation, or path-independent (holonomic) models practically admissible sometimes under proportional loading monotonically increasing in time; time-independence or viscoplastic time-

[1] Dedicated to Professor Kaspar Willam on the occasion of his 60 th anniversary.

[2] Department of Structural Engineering, Technical University (Politecnico) of Milan, Italy.

[3] On leave from Department of Mechanics, College of Science, Northeastern University, Shenyang, China.

dependence.

In this paper piece-wise linear (PWL) time-independent elastic-plastic-softening and rigid-plastic-softening interface models are developed and investigated as for their potentialities and limitations in the approximate, engineering-oriented description of nonlinear behaviours localised on discontinuity loci Γ_d.

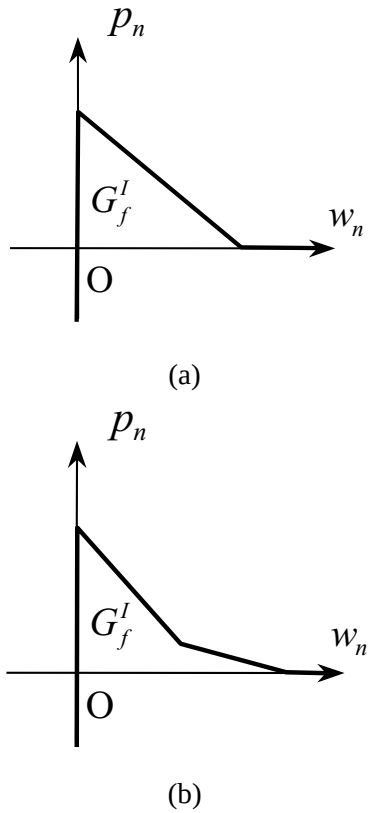

Figure 1 : Piecewise linear cohesive crack models for mode I quasi-brittle fracture.

The antecedents and the possible advantages which motivate the present study can be outlined as follows.

(a) For the simulation of quasi-brittle fracture processes, at present the most widely used approach appears to rest on a PWL cohesive crack model in mode I with one or two softening linear branches (Fig. 1), i.e. governed by two or four parameters, respectively (see e.g. Guinea, Planas and Elices (1994), Karihaloo (1995), Maier and Comi (2000)). The generalisation of this model to mixed mode fracture, by preserving its PWL features, is of obvious interest, but not yet developed so far, to the writers' knowledge.

(b) Limit and shakedown analyses based on PWL elastic-plastic material models are popular since long time, because their consequent reduction to linear programming. In fact, PWL approximations of constitutive laws have been adopted for "direct" (non step-by-step) ultimate limit-state analyses of a variety of structural systems, namely: steel and reinforced concrete frames; earth slopes; shallow foundations and other geotechnical situations; ductile, metal matrix composites; large dams, also when they are interpreted as poroplastic in view of diffused cracking (see survey Maier, Carvelli and Cocchetti (2000)). However, limit and shakedown analysis rest on the constitutive stability hypothesis expressed by Drucker's postulate that rules out softening, which is instead of paramount importance in the present context.

(c) The rate flow rules of plasticity are centred on, and characterised by, a nonlinear relationship called linear complementarity problem (LCP). Mechanically, it expresses "Prager consistency" (which can be regarded as a manifestation of irreversibility): for each active yielding mode, either the (non positive) yield function rate or the (nonnegative) plastic multiplier rate, or both, must vanish. Mathematically, when the current stress state belongs to the yield locus, say to the intersection ("corner") of say n_y yield surfaces, the two sign-constrained n_y-vectors of the relevant yield function rates and of the plastic multiplier rates are orthogonal and related to each other also through a suitably arranged linear expression of the former vector, where the stress rates (or the strain rates) are regarded as given. A peculiar feature of PWL models is that the LCP construct carries over from the flow rules in rates to finite-step formulations for time integration (which always rests on a step-wise holonomic interpretation of the non-holonomic constitutive model) and, further, to single-step, holonomic versions of the constitution, in the spirit of the "deformation theory" of plasticity. Holonomic plasticity (conceivable as a special case of nonlinear elasticity) is applicable in practice when local unstressing is unlikely to occur, typically in structures under monotonic proportional loading, see e.g. De Donato and Maier (1976), Lloyd Smith (1990), Maier (1970, 1976). Under the frequently reasonable hypothesis of infinitesimal strains and linear kinematics, the LCP pattern carries over to the overall structural analysis, if this is performed on the basis of a space discretisation, say by a finite element or boundary element method. The above potentially unifying and computationally beneficial role of PWL-LCP models in engineering plasticity

emerges more or less explicitly in a fairly abundant literature, see e.g. the book edited by Lloyd Smith (1990), mostly again ruling out softening (with a few exceptions, such as Bolzon, Maier and Tin-Loi (1995, 1997)). For interfaces, however, softening represents a material instability which plays a crucial role.

(d) From the standpoint of computational efficiency, the PWL-LCP formulations exhibit the "contra" of the significant increase in the number of yield modes and, hence, of variables. For the material description in 2D or 3D problems, this "con" may prevail over the pros of reduction from nonlinear programming (NLP) to linear programming (LP) in limit analysis, and of the systematic use of LCP algorithms, instead of nonlinear complementarity problem (NLCP) or other (say Newton-Raphson type) algorithms. However, for interfaces of concern here, PWL models involve traction and displacement vectors with two or, at most, three components; moreover, in general, provisions apt to drop presumably inactive yield modes and relevant variables can easily be devised and implemented, see e.g. Tin-Loi (1990), as shown in a forthcoming paper on overall analysis of concrete dams.

1.2 Objectives and organisation of this paper

Motivated by the remarks which precede, the topics to be considered herein and the aims to be pursued are as follows.

Piecewise linearisation IM will be developed for softening and multicomponent situations (mixed modes) combined, thus relaxing the restrictions of PWL IM to mixed modes with material stability or to mode I with softening (Section 2).

The close links between holonomic and non-holonomic PWL models will be pointed out together with "exact" and approximate time integration procedures proposed in Section 3.

Two kinds of PWL IMs are formulated in Section 4 and specialised and discussed through numerical tests in Section 5: a PWL IM for frictional contact; a PWL IM intended to simulate fracture processes in quasi-brittle structures and debonding in laminates and composites at the microscale. Since LCP will be shown to be the recurrent, unifying mathematical construct, a typical algorithm available nowadays for solving general LCP is briefly outlined in Section 6. Section 7 gathers some conclusions in view of the practical usage of PWL models in overall analyses of concrete dams and other structures.

Notation Matrix notation is adopted throughout. Matrix and vectors are represented by bold-face characters. Transposition is indicated by superscript T. A dot marks rate, i.e. derivative with respect to ordering, not necessarily physical, time t. Vector inequalities apply componentwise

2 Piecewise linear interface models

2.1 General elastic-plastic interface models.

The locus of possible discontinuities for the displacement field in a solid is assumed henceforth to be represented by a "smooth" surface Γ_d. In view of the assumed smoothness, at any point $\mathbf{x}$ of Γ_d a normal and two tangential directions (say, along the directions of the principal curvatures) can be defined and taken as unit vectors of a Cartesian reference frame. In this reference, the displacement jump $\mathbf{w} = \{w_n\, w_{t1}\, w_{t2}\}^T$ and the traction $\mathbf{p} = \{p_n\, p_{t1}\, p_{t2}\}^T$ across Γ_d are defined, so that the scalar-product $\mathbf{p}^T\dot{\mathbf{w}}$ represents the energy rate (stored or dissipated) per unit surface on Γ_d in $\mathbf{x}$.

Any (generally path– and time–dependent) relationship between the above two vectors is understood herein as interface model (IM) or interface "law". The particular, but broad, class of inviscid, path-dependent (non-holonomic) IM can be represented by the following set of relationships in a format which is customary in engineering plasticity of materials and structures (see e.g. Maier and Frangi (1998)):

$$\mathbf{p} = \frac{\partial E\,(\mathbf{w}^e)}{\partial \mathbf{w}^e}, \qquad \mathbf{w} = \mathbf{w}^e + \mathbf{w}^p \tag{1}$$

$$\boldsymbol{\varphi} = \boldsymbol{\varphi}(\mathbf{p},\boldsymbol{\chi}), \qquad \boldsymbol{\Psi} = \boldsymbol{\Psi}(\mathbf{p},\boldsymbol{\chi}) \tag{2}$$

$$\boldsymbol{\chi} = \frac{\partial U\,(\boldsymbol{\eta})}{\partial \boldsymbol{\eta}} \tag{3}$$

$$\dot{\mathbf{w}}^p = \frac{\partial \boldsymbol{\Psi}^T}{\partial \mathbf{p}}\dot{\boldsymbol{\lambda}}, \qquad \dot{\boldsymbol{\eta}} = -\frac{\partial \boldsymbol{\Psi}^T}{\partial \boldsymbol{\chi}}\dot{\boldsymbol{\lambda}} \tag{4}$$

$$\boldsymbol{\varphi} \le \mathbf{0}, \qquad \dot{\boldsymbol{\lambda}} \ge \mathbf{0}, \qquad \boldsymbol{\varphi}^T\dot{\boldsymbol{\lambda}} = 0 \tag{5}$$

Equations (1a) and (1b) express (generally nonlinear) elasticity through a strictly convex elastic potential E and additivity of elastic $\mathbf{w}^e$ and plastic $\mathbf{w}^p$ relative displacements, respectively. Damage, in the sense of continuum damage mechanics, might be allowed for by assuming

that the elastic potential E depends also on some of the kinematic internal variables collected in vector $\boldsymbol{\eta}$.

Yield functions and plastic potentials (gathered in n_y–vectors $\boldsymbol{\varphi} = \{\varphi_1, ..., \varphi_y\}^T$ and $\boldsymbol{\Psi} = \{\Psi_1, ..., \Psi_y\}^T$) are introduced in Eq.2 as differentiable ("smooth") and convex (but not necessarily strictly convex) functions of tractions and of static internal variables collected in the n_y–vector $\boldsymbol{\chi}$. This vector acquires in Eq.3 the meaning of gradient of another potential function U (interpreted as part of Helmholtz free energy locked-in by microscale re-arrangements) with respect to the kinematic variable vector $\boldsymbol{\eta}$ which is work-conjugate to $\boldsymbol{\chi}$.

The evolution of the inelastic ("plastic") displacement jumps $\mathbf{w}^p$ and of the internal variables $\boldsymbol{\eta}$ is governed by Eq.4 and by the complementarity relationship Eq. 5.

The rate relationship (or "flow laws") implied by Eqs.1–5 at a given state $(\hat{\mathbf{p}}, \hat{\boldsymbol{\eta}})$ read:

$$\dot{\boldsymbol{\varphi}}' = \frac{\partial \boldsymbol{\varphi}'(\hat{\mathbf{p}}, \hat{\boldsymbol{\chi}})}{\partial \mathbf{p}^T} \dot{\mathbf{p}} - \mathbf{H}(\hat{\mathbf{p}}, \hat{\boldsymbol{\eta}}) \dot{\boldsymbol{\lambda}}' \leq \mathbf{0}, \quad \dot{\boldsymbol{\lambda}}' \geq \mathbf{0}, \quad \dot{\boldsymbol{\varphi}}'^T \dot{\boldsymbol{\lambda}}' = 0 \tag{6}$$

where ("hardening matrix"):

$$\mathbf{H}(\hat{\mathbf{p}}, \hat{\boldsymbol{\eta}}) = \frac{\partial \boldsymbol{\varphi}'(\hat{\mathbf{p}}, \hat{\boldsymbol{\chi}})}{\partial \boldsymbol{\chi}^T} \frac{\partial^2 U(\hat{\boldsymbol{\eta}})}{\partial \boldsymbol{\eta} \partial \boldsymbol{\eta}^T} \frac{\partial \boldsymbol{\Psi}'(\hat{\mathbf{p}}, \hat{\boldsymbol{\chi}})^T}{\partial \boldsymbol{\chi}} \tag{7}$$

For assigned traction rates $\dot{\mathbf{p}}$, Eqs.6 and 7 represent a LCP in $\dot{\boldsymbol{\varphi}}'$ and $\dot{\boldsymbol{\lambda}}'$, where primes denote the subvectors of $\dot{\boldsymbol{\varphi}}'$ and $\dot{\boldsymbol{\lambda}}'$, respectively, pertaining to the yield modes which are "active" at $(\hat{\mathbf{p}}, \hat{\boldsymbol{\eta}})$, i.e. whose yield functions vanish there $(\boldsymbol{\varphi}' = \mathbf{0})$.

Eqs.1–7 can be regarded as the "direct" formulation of a path-dependent (irreversible, non-holonomic) IM, briefly as a relationship of the type: $\mathbf{w}(t) = f[\mathbf{p}(\tau), 0 \leq \tau \leq t]$. An "inverse" formulation for given discontinuity history, i.e. $\mathbf{p}(t) = g[\mathbf{w}(\tau), 0 \leq \tau \leq t]$, can be achieved by traditional provisions, here omitted for brevity.

Consistently with the above IM, the power per unit area reads:

$$\dot{\Pi} \equiv \mathbf{p}^T \dot{\mathbf{w}} = \mathbf{p}^T \dot{\mathbf{w}}^e + \mathbf{p}^T \dot{\mathbf{w}}^p = \dot{E} + \dot{U} + \dot{D} \tag{8}$$

where the specific dissipation $\dot{D}$ is subjected to the usual thermo-dynamical requirement of nonnegativeness:

$$\dot{D} = \mathbf{p}^T \dot{\mathbf{w}}^p - \boldsymbol{\chi}^T \dot{\boldsymbol{\eta}} \geq 0 \tag{9}$$

In plasticity, stability is characterised by nonnegativeness of the second order work $\delta^2\Pi$ for all kinematic disturbances, namely, in the present case, by the condition:

$$\delta^2 \Pi = \frac{1}{2} \dot{\mathbf{w}}^T \dot{\mathbf{p}}(\dot{\mathbf{w}}) \, \delta t^2 \geq 0, \forall \dot{\mathbf{w}} \tag{10}$$

Using Eqs.1–5 and 6c, we can write:

$$\delta^2 \Pi = \frac{\delta t^2}{2} \left[\dot{\mathbf{w}}^T \mathbf{D} \dot{\mathbf{w}}^T - \dot{\mathbf{w}}^T \mathbf{D} \frac{\partial \boldsymbol{\Psi}^T}{\partial \mathbf{p}} \dot{\boldsymbol{\lambda}}(\dot{\mathbf{w}}) \right] \tag{11}$$

The tangential elastic stiffness matrix (symmetric and positive-definite in view of the strict convexity of E) reads:

$$\mathbf{D}(\mathbf{w}^e) \equiv \frac{\partial^2 E(\mathbf{w}^e)}{\partial \mathbf{w}^e \partial \mathbf{w}^{eT}} \tag{12}$$

Drucker's stability postulate, can be formulated in the following form.

If for any traction path Γ starting from any state $(\mathbf{p}^*, \boldsymbol{\eta}^*)$ such that $\boldsymbol{\varphi}(\mathbf{p}^*, \boldsymbol{\eta}^*) \leq \mathbf{0}$ it is verified that:

$$\int_\Gamma (\mathbf{p} - \mathbf{p}^*)^T \dot{\mathbf{w}} dt \geq 0 \tag{13}$$

then the material is stable.

This strong "stability postulate" could be easily proven to imply: (*i*) associativity, namely $\boldsymbol{\varphi} = \boldsymbol{\psi}$; (*ii*) convexity of any current elastic domain $\boldsymbol{\varphi} \leq \mathbf{0}$; (*iii*) stability in the sense of Eq.10. Variational properties of systems with nonlinearity due to general IM have been recently established in Carini and Maier (2000).

2.2 Piecewise linear elastic-plastic models in general

The category of IMs described in the preceding Subsection is specialised below to the PWL class by means of the following restrictive assumptions: (*a*) the elastic strain energy E is a homogeneous quadratic function of $\mathbf{w}^e$, so that its Hessian Eq.12 becomes the elastic stiffness matrix $\mathbf{D}$; (*b*) also the stored free energy U is homogeneous quadratic function of $\boldsymbol{\eta}$ defined by a constant

matrix **C**; (*c*) the yield functions in $\boldsymbol{\varphi}$ are linear in their arguments $(\mathbf{p},\boldsymbol{\chi})$, so that their gradients are constant (and will be gathered henceforth in matrix $[\mathbf{N},\mathbf{N}_\chi]$; (*d*) all the plastic potentials are linear in $(\mathbf{p},\boldsymbol{\chi})$, with constant gradients collected, say, in matrix $[\mathbf{V},\mathbf{V}_\chi]$.

In view of the above assumptions and new symbols, Eqs. 1–5 specialise to:

$$\mathbf{p}=\mathbf{D}\mathbf{w}^e, \qquad \mathbf{w}=\mathbf{w}^e+\mathbf{w}^p \tag{14}$$

$$\boldsymbol{\varphi}=\mathbf{N}^T\mathbf{p}+\mathbf{N}_\chi^T\boldsymbol{\chi}-\mathbf{Y}, \qquad \boldsymbol{\Psi}=\mathbf{V}^T\mathbf{p}+\mathbf{V}_\chi^T\boldsymbol{\chi} \tag{15}$$

$$\chi=\mathbf{C}\boldsymbol{\eta}, \qquad \mathbf{w}^p=\mathbf{V}\boldsymbol{\lambda}, \qquad \boldsymbol{\eta}=-\mathbf{V}_\chi\boldsymbol{\lambda} \tag{16}$$

$$\boldsymbol{\varphi}\le\mathbf{0}, \qquad \dot{\boldsymbol{\lambda}}\ge\mathbf{0}, \qquad \boldsymbol{\varphi}^T\dot{\boldsymbol{\lambda}}=0 \tag{17}$$

Here the constant vector **Y** can be regarded as collecting "yield limits", since the *i*-th component of it represents the original distance of the *i*-th yield plane from the origin in the traction space after a normalisation which makes all columns in matrix **N** to become unit vectors in space **p** (the same is herein assumed for matrix **V**). It is worth noting that the above linearisations, namely assumptions (*b*), (*c*) and (*d*), permit to substitute for $\boldsymbol{\chi}$ and $\boldsymbol{\eta}$ the (time-integrated) plastic multipliers $\boldsymbol{\lambda}$ which thus acquire also the role of internal variables.

If the input is represented by a given time history of traction **p**(t), then the response in terms of displacement discontinuity **w**(t) through the PWL IM, Eqs.14–17, turns out to be governed by the following relations ("direct" PWL IM formulation):

$$\boldsymbol{\varphi}=\mathbf{N}^T\mathbf{p}(t)-\mathbf{H}\boldsymbol{\lambda}-\mathbf{Y}\le\mathbf{0}, \quad \dot{\boldsymbol{\lambda}}\ge\mathbf{0}, \quad \boldsymbol{\varphi}^T\dot{\boldsymbol{\lambda}}=0 \tag{18}$$

$$\mathbf{w}(t)=\mathbf{D}^{-1}\mathbf{p}+\mathbf{V}\boldsymbol{\lambda} \tag{19}$$

where "hardening matrix" **H**, Eq.7, now is constant and reads:

$$\mathbf{H}=\mathbf{N}_\chi^T\mathbf{C}\mathbf{V}_\chi \tag{20}$$

Similarly, the "inverse" formulation of the PWL IM, governing the traction response **p**(t) to an assigned path of relative displacements **w**(t), can be easily seen to materialise in the relationship:

$$\boldsymbol{\varphi}=\mathbf{N}^T\mathbf{D}\mathbf{w}(t)-\mathbf{K}\boldsymbol{\lambda}-\mathbf{Y}\le\mathbf{0}, \quad \dot{\boldsymbol{\lambda}}\ge\mathbf{0}, \quad \boldsymbol{\varphi}^T\dot{\boldsymbol{\lambda}}=0 \tag{21}$$

$$\mathbf{p}(t)=\mathbf{D}\mathbf{w}-\mathbf{D}\mathbf{V}\boldsymbol{\lambda} \tag{22}$$

having set:

$$\mathbf{K}\equiv\mathbf{H}+\mathbf{N}^T\mathbf{D}\mathbf{V} \tag{23}$$

In both the direct and the inverse PWL IM, all nonlinearities are confined to Eqs.18 and 21, respectively. When the rate vector $\dot{\boldsymbol{\lambda}}(t)$ and, hence, $\boldsymbol{\lambda}(t)$ are computed through them, then the response **w**(t) or **p**(t) results from explicit linear transforms, Eq.19 or 22, respectively.

In terms of rates (i.e. of infinitesimal increments) starting from a state $\left\{\hat{\mathbf{p}},\hat{\boldsymbol{\lambda}}\right\}$ where only a subset of yield planes are active (marked by a prime), Eqs.18 and 21 generate straightforwardly the following direct and inverse flow rules, respectively, in the LCP format:

$$\dot{\boldsymbol{\varphi}}'=\mathbf{N}'^T\dot{\mathbf{p}}-\mathbf{H}'\dot{\boldsymbol{\lambda}}'\le\mathbf{0}, \quad \dot{\boldsymbol{\lambda}}'\ge\mathbf{0}, \quad \dot{\boldsymbol{\varphi}}'^T\dot{\boldsymbol{\lambda}}'=0 \tag{24}$$

$$\dot{\boldsymbol{\varphi}}'=\mathbf{N}'^T\mathbf{D}\dot{\mathbf{w}}-\mathbf{K}'\dot{\boldsymbol{\lambda}}'\le\mathbf{0}, \quad \dot{\boldsymbol{\lambda}}'\ge\mathbf{0}, \quad \dot{\boldsymbol{\varphi}}'^T\dot{\boldsymbol{\lambda}}'=0 \tag{25}$$

Clearly, Eq.24 is a trivial specialisation of Eq.6, with the new symbols for the coefficient matrices. All these matrices are now always submatrices of their counterparts (defined once for all) in the full IM, Eqs.14–17, and, hence, must be singled out in them on the basis of the current state $\left\{\hat{\mathbf{p}},\hat{\boldsymbol{\lambda}}\right\}$, but otherwise they do not depend on it. A similar remark obviously holds for the inverse flow rules, Eq.25, the counterpart of which in the more general context of Subsection 2.1 was not written for brevity

2.3 Remarks

The main peculiar feature of PWL IMs of concern herein is represented by the fact that the yield surfaces in the 3D traction space are "yield planes", which may merely translate at yielding and "interact" (in the sense that the activation of one can induce others to translate). Clearly, these motions and interactions are governed by the hardening matrix **H**. In fact, if matrix **N** is normalised (in the sense that each column of it, say vector $\mathbf{N}_r$, r = 1,..., n_y, represents the outward normal unit vector), then the distance of the yield plane from the origin, denoting by $\mathbf{H}_r$ the r-th row of **H**, reads:

$$Y_r+\mathbf{H}_r\boldsymbol{\lambda}=Y_r', \qquad (r=1,\ldots,n_y) \tag{26}$$

The following circumstances are worth noticing on matrix **H** (of order n_y).

If **H** is diagonal, there is no interaction among yield planes ("Koiter's rule" of noninteracting yield modes, in the jargon of classical plasticity).

In classical plasticity, Prager's kinematic hardening and isotropic hardening mean rigid-body translation and, respectively, shape-preserving homothetic expansion of the entire yield locus. In the PWL context, such restrictive assumptions reduce drastically (to a single one, say h and k, respectively) the available hardening/softening parameters and imply (as shown in Maier (1970) for materials) the following specialisation of matrix **H**, respectively:

$$\mathbf{H} = k\mathbf{N}^T\mathbf{N}, \qquad \mathbf{H} = h\mathbf{Y}\left\{\frac{1}{Y_1}, \quad \ldots, \quad \frac{1}{Y_{n_y}}\right\} \tag{27}$$

Rigid-plastic PWL IMs can be regarded as the limit case for increasing elastic stiffness, i.e. for $s \to \infty$ having assumed $\mathbf{D} = s\,\mathbf{D}_0$. The direct formulation, Eqs.18 - 19, straightforwardly specialises to a rigid-plastic one just by dropping the elastic addend in Eq.19. Clearly, not so in the inverse formulation, which gives rise to the following remarks.

In interface models, elasticity has usually a computational role rather than a physical meaning. In the present PWL IM, a large scalar s acts as penalisation factor against compenetrations (like in the "smooth" exponential IM proposed in Xu and Needleman (1994)).

The popular PWL IMs for mode I cohesive crack model of quasi-brittle fracture (Fig. 1) are rigid-plastic. It is worth noting that the LCP descriptions established in Bolzon, Maier and Tin-Loi (1995), Maier and Comi (2000) for mode I are substantially different from the present LCP description. In fact, w_n is there a sign-constrained variable like the plastic multipliers (or "auxiliary variables"), not a free (and possibly input) variable like here.

Clearly, convexity of all current elastic domains implied by Drucker's postulate, Eq.13, is intrinsic in the PWL approximation, since all yield modes are represented (in 3D contexts) by translating and interacting yield planes associated to half-spaces, the intersection of which is a convex polyhedron.

The internal static and kinematic variables have been assumed by Eqs.3 and 16a to be related to each other through a potential U which is quadratic in PWL IM and has the meaning of density of recoverable energy stored at the microscale. Matrix **C**, being Hessian of U, turns out to be symmetric (and constant in PWL IM). Then associativity in the sense of $\mathbf{N}_\chi = \mathbf{V}_\chi$ which does not imply associativity in the **p** space, as usually understood in plasticity) implies the symmetry of the hardening matrix **H**. However, nonsymmetric **C** and, hence, nonsymmetric **H** in associative cases (even if fully associative, namely for $\mathbf{N}_\chi = \mathbf{V}_\chi$ and $\mathbf{N} = \mathbf{V}$) are quite admissible, since nondissipative rearrangement at the microscale is an assumption, not a thermodynamic law of nature.

In order to evidence the meaning and the instabilising effects of softening in PWL IM, the second order work $\delta^2\Pi$ through easy manipulations of Eqs. 18-20, can be expressed in the following form, alternative to a straightforward PWL specialisation of Eq.11:

$$\delta^2\Pi = \frac{\delta t^2}{2}\left[\dot{\mathbf{w}}^{eT}\mathbf{D}\dot{\mathbf{w}}^e + \dot{\boldsymbol{\lambda}}^T\mathbf{H}\dot{\boldsymbol{\lambda}} + \dot{\mathbf{p}}^T\left(\frac{\partial\boldsymbol{\Psi}^T}{\partial\mathbf{p}} - \frac{\partial\boldsymbol{\varphi}^T}{\partial\mathbf{p}}\right)\dot{\boldsymbol{\lambda}}\right] \tag{28}$$

Since the elastic strain energy E is assumed as strictly convex (and, hence, its Hessian matrix in Eq.12 as positive definite), associativity ($\boldsymbol{\varphi} = \boldsymbol{\psi}$) implies that instability may occur only when U is nonconvex (i.e., **H** is nondefinite): a circumstance which means softening behaviour and may have crucial consequences on the overall structural response to loads (see e.g. Bolzon, Maier and Tin-Loi (1997), Cen and Maier (1992)).

3 Time integration procedures for piecewise linear models

3.1 Exact integration

Let us now focus on the step-by-step time integration of a PWL IM. To this purpose, as usual in computational plasticity, we consider the given traction path $\hat{\mathbf{p}}(t)$ as a sequence of data $\hat{\mathbf{p}}_0, \hat{\mathbf{p}}_1, \ldots, \hat{\mathbf{p}}_n, \hat{\mathbf{p}}_{n+1}, \ldots$, in correspondence with a sequence of instants $t = 0, t_1, \ldots, t_n, t_{n+1}, \ldots$, assuming a proportional monotonic variation of the input quantity (marked by a cap) along each time interval, namely over $\Delta t_n = t_{n+1} - t_n$:

$$\hat{\mathbf{p}}(t|t_n \le t \le t_{n+1}) = \hat{\mathbf{p}}_n + (t - t_n)\dot{\hat{\mathbf{p}}}_n\,, \tag{29a}$$

$$\dot{\hat{\mathbf{p}}}_n = \frac{\Delta\hat{\mathbf{p}}_n}{\Delta t_n} = \frac{(\hat{\mathbf{p}}_{n+1} - \hat{\mathbf{p}}_n)}{\Delta t_n} \tag{29b}$$

Under this weak assumption, the following procedure of "exact" integration can be devised as a computationally advantageous consequence of the particular properties of PWL modelling, see e.g. Maier (1976), Nappi and Perego (1988). The exact procedure is outlined phase-wise and justified below. Barred symbols will denote quantities which have already been computed. Single and double primes will mark the subvectors in $\boldsymbol{\varphi}$ and $\boldsymbol{\Psi}$ (and consequently the submatrices in $\mathbf{N}$ and $\mathbf{H}$) which correspond to yield planes currently active ($\boldsymbol{\varphi}' = \mathbf{0}$) and non active ($\boldsymbol{\varphi}'' < \mathbf{0}$), respectively.

(a) At the (known) starting state $\left(\hat{\mathbf{p}}_n, \overline{\boldsymbol{\lambda}}_n\right)$ solve the LCP, Eq.24, of the flow rule for given rate $\dot{\hat{\mathbf{p}}}$. Let $\overline{\dot{\boldsymbol{\lambda}}}_1'$ be the (or a) solution of this first problem in rates, having understood that $\overline{\dot{\boldsymbol{\lambda}}}_1'' = \mathbf{0}$.

(b) Noting that the LCP of Eq.24 is linear homogeneous in an amplifier Δt of both data and variables, compute the value Δt_1 such that a new yield plane (or more than one) is "activated", i.e. is reached by point $\hat{\mathbf{p}}_n + \dot{\hat{\mathbf{p}}}_n \Delta t$:

$$\Delta t_1 = \max\left\{\Delta t \left| \boldsymbol{\varphi}''(\Delta t) \leq \mathbf{0} \right.\right\} \tag{30}$$

where, with self-evident meaning of the symbols (in particular: "$\mathbf{H}$' is the submatrix of $\mathbf{H}$ formed by the intersection of its rows corresponding to $\boldsymbol{\varphi}'' < \mathbf{0}$, with its columns corresponding to $\boldsymbol{\varphi}' = \mathbf{0}$):

$$\boldsymbol{\varphi}''(\Delta t) = \overline{\boldsymbol{\varphi}}_n'' + \left(\mathbf{N}''^T \dot{\hat{\mathbf{p}}} - {}''\mathbf{H}' \overline{\dot{\boldsymbol{\lambda}}}_1'\right) \Delta t \tag{31}$$

(c) In view of the new active and new inactive yield modes, re-arrange vectors and matrices by re-decomposition into primed and double primed portions. Thereafter go to (a) and repeat the operative sequence (a) and (b).

(d) Stop when $\Delta t_1 + \Delta t_2 + \ldots + \Delta t_l \geq \Delta t_n$, and, in the case of strict inequality, reduce the last substep Δt_l, so that the equality holds.

Summing up the results of all substeps, the plastic multiplier increment due to the assigned $\Delta \hat{\mathbf{p}}_n$ turns out to be:

$$\Delta\boldsymbol{\lambda} = \left\{\begin{matrix}\overline{\dot{\boldsymbol{\lambda}}}_1' \\ \overline{\dot{\boldsymbol{\lambda}}}_1'' = \mathbf{0}\end{matrix}\right\}\Delta t_1 + \left\{\begin{matrix}\overline{\dot{\boldsymbol{\lambda}}}_2' \\ \overline{\dot{\boldsymbol{\lambda}}}_2'' = \mathbf{0}\end{matrix}\right\}\Delta t_2 + \ldots + \left\{\begin{matrix}\overline{\dot{\boldsymbol{\lambda}}}_l' \\ \overline{\dot{\boldsymbol{\lambda}}}_l'' = \mathbf{0}\end{matrix}\right\}\Delta t_l \tag{32}$$

which defines through Eq.19 the response $\Delta\mathbf{w}$ ("exact" according to the PWL model).

Clearly, the same algorithm applies to the inverse PWL IM, Eqs.21-22, i.e. for input $\hat{\mathbf{w}}(t)$ and response $\mathbf{p}$(t). With reference to the inverse model, and to the n-th proportional input step $\dot{\hat{\mathbf{w}}}_n \Delta t_n$, the "exact" algorithm is described below again for later use.

(a) At the beginning of the i-th substep (i = 1,2,...) within the step n over the time interval Δt_n, consider the state $\left\{\hat{\mathbf{w}}_i, \overline{\boldsymbol{\lambda}}_i\right\}$ reached so far and the consequent n_y-vector $\overline{\boldsymbol{\varphi}}_i$ of yield functions. Distinguish active (') from inactive (") yield models at t_i and partition vectors and matrices accordingly:

$$\overline{\boldsymbol{\varphi}}_i = \left\{\begin{matrix}\overline{\boldsymbol{\varphi}}_i' = \mathbf{0} \\ \overline{\boldsymbol{\varphi}}_i'' < \mathbf{0}\end{matrix}\right\}, \quad \dot{\boldsymbol{\lambda}}_i = \left\{\begin{matrix}\dot{\boldsymbol{\lambda}}_i' \geq \mathbf{0} \\ \dot{\boldsymbol{\lambda}}_i'' = \mathbf{0}\end{matrix}\right\} \tag{33}$$

$$\mathbf{N}_i = [\mathbf{N}'\,\mathbf{N}'']_i, \quad \mathbf{V}_i = [\mathbf{V}'\,\mathbf{V}'']_i, \quad \mathbf{K}_i = \begin{bmatrix}\mathbf{K}' & '\mathbf{K}'' \\ {}''\mathbf{K}' & \mathbf{K}''\end{bmatrix}_i \tag{34}$$

(b) Solve the following LCP in $\left\{\dot{\boldsymbol{\varphi}}_i', \dot{\boldsymbol{\lambda}}_i'\right\}$ to obtain $\left\{\overline{\boldsymbol{\varphi}}_i', \overline{\dot{\boldsymbol{\lambda}}}_i'\right\}$:

$$\dot{\boldsymbol{\varphi}}_i' = \mathbf{N}_i'^T \mathbf{D}\,\dot{\hat{\mathbf{w}}}_n - \mathbf{K}'_i \dot{\boldsymbol{\lambda}}_i' \leq \mathbf{0}, \quad \dot{\boldsymbol{\lambda}}_i' \geq \mathbf{0}, \quad \dot{\boldsymbol{\varphi}}_i'^T \dot{\boldsymbol{\lambda}}_i' = 0 \tag{35}$$

(c) Solve the LP problem, thus obtaining Δt_i:

$$\Delta t_i = \max\left\{\Delta t \left| \hat{\boldsymbol{\varphi}}_i'' + \left(\mathbf{N}''^T_i \mathbf{D}\,\dot{\hat{\mathbf{w}}}_n - {}''\mathbf{K}'_i \overline{\dot{\boldsymbol{\lambda}}}_i'\right)\Delta t \leq \mathbf{0}\right.\right\} \tag{36}$$

(d) Update the vectors:

$$\overline{\boldsymbol{\varphi}}_{i+1} = \overline{\boldsymbol{\varphi}}_i + \dot{\overline{\boldsymbol{\varphi}}}_i \Delta t_i, \qquad \overline{\boldsymbol{\lambda}}_{i+1} = \overline{\boldsymbol{\lambda}}_i + \overline{\dot{\boldsymbol{\lambda}}}_i \Delta t_i \tag{37}$$

(e) Go to (a) and re-arrange according to the criteria specified there.

(f) Stop when $\sum_{i}^{l} \Delta t_i = \Delta t_n$, by scaling down the last Δt_i if necessary; then accumulate the results of the substep sequence to obtain:

$$\Delta \mathbf{p}_n = \mathbf{D}\Delta\hat{\mathbf{w}}_n - \mathbf{DV}\sum_{i=1}^{l} \left\{ \begin{array}{l} \overline{\overline{\boldsymbol{\lambda}}}'_i \\ \overline{\overline{\boldsymbol{\lambda}}}''_i = \mathbf{0} \end{array} \right\} \Delta t_i \tag{38}$$

3.2 Stepwise holonomic integration

The exact integration which precedes exhibits the peculiar feature that the number of substeps Δt_i (i = 1, 2, ..., l) within each given Δt_n cannot be chosen a priori, but depends on the model and on the input path. Clearly, this fact becomes computationally disadvantageous in structural analysis, when yield modes are simultaneously active in many points on the displacement discontinuity locus Γ_d according to the adopted space discretisation on it.

In order to avoid the consequent, possibly drastic, reduction of substep amplitudes Δt_i, let us assume that the path-dependence does not hold within each step; in other terms, the intrinsic irreversibility of the model is accounted for only in updating the internal variables at the transition from step to step. Such frequent "stepwise holonomic" interpretation of the evolution of a dissipative systems, if applied to the PWL IMs in point, leads to a step-governing relation set once again in LCP format (like above for the flow rules).

In fact, with reference to the inverse model only (in view of the formal similarity with the direct model), and to the assigned step $\Delta\hat{\mathbf{w}}_n$ over the time interval $\Delta t_n = t_{n+1} - t_n$, we can write the following LCP in variables $\{\Delta\boldsymbol{\varphi}_n, \Delta\boldsymbol{\lambda}_n\}$:

$$\boldsymbol{\varphi}_n + \Delta\boldsymbol{\varphi}_n = \mathbf{N}^T\mathbf{D}\cdot(\hat{\mathbf{w}}_n + \Delta\hat{\mathbf{w}}_n) +$$

$$-\mathbf{K}\boldsymbol{\lambda}_n - \mathbf{K}\Delta\boldsymbol{\lambda}_n - \mathbf{Y} \leq \mathbf{0}, \qquad \Delta\boldsymbol{\lambda}_n \geq \mathbf{0} \tag{39}$$

$$(\boldsymbol{\varphi}_n + \Delta\boldsymbol{\varphi}_n)^T \Delta\boldsymbol{\lambda}_n = 0 \tag{40}$$

supplemented by the application of Eq.22 apt to linearly update the traction response as soon as $\Delta\hat{\boldsymbol{\lambda}}_n$ is computed:

$$\Delta\mathbf{p}_n = \mathbf{D}\Delta\hat{\mathbf{w}}_n - \mathbf{DV}\Delta\boldsymbol{\lambda}_n \tag{41}$$

3.3 Remarks

The meaning and implications of the above LCP in finite increments are clarified by the following remarks.

(a) Since the model relations Eq. 21a and Eq. 21b hold at any time, Eqs.39 are rigorous consequences of them. Not so the complementarity Eq.40, which embodies an assumption intended to establish a path-independent link between input and output finite increments in the step Δt_n. It is worth noting that such an assumption is generally an approximation, but is exactly fulfilled in the case of "regularly progressive yielding" (RPY), i.e. no local unstressing over Δt_n. This RPY notion formally means:

$$\text{if } \dot{\lambda}_r(t^*) > 0, \text{ then } \varphi_r(t) = 0, \left\{ \begin{array}{l} \forall t : t_n \leq t^* \leq t \leq t_{n+1} \\ r = 1, \ldots, n_y \end{array} \right. \tag{42}$$

and thus the sheer existence of any RPY path over Δt_n is seen to imply Eq.40.

(b) Now let the further assumption of "no new yielding" over Δt_n be admitted in the (undefined) actual path over Δt_n; formally:

$$\text{if } \varphi_r(t_n) < 0, \text{ then } \dot{\lambda}_r(t) = 0, \left\{ \begin{array}{l} \forall t : t_n \leq t \leq t_{n+1} \\ r = 1, \ldots, n_y \end{array} \right. .$$

Then $\boldsymbol{\varphi}_n^T\Delta\boldsymbol{\lambda} = 0$, and, hence, Eqs.39 and 41 generate the following LCP:

$$\Delta\boldsymbol{\varphi}_n = \mathbf{N}^T\mathbf{D}\Delta\hat{\mathbf{w}}_n - \mathbf{K}\Delta\boldsymbol{\lambda}_n \leq \mathbf{0}, \quad \Delta\boldsymbol{\lambda}_n \geq \mathbf{0}, \quad \Delta\boldsymbol{\varphi}_n^T\Delta\boldsymbol{\lambda}_n = 0 \tag{43}$$

(c) In computational plasticity, quasi-static and dynamic time-stepping analyses of structures are always stepwise holonomic and are usually carried out by finite difference schemes resting on the following assumptions: (*i*) the constitutive law is enforced only at some instant $t_\alpha = t_n + \rho\Delta t_n$, $0 \leq \rho \leq 1$; (*ii*) all variables vary linearly over the time interval Δt_n; (*iii*) the variation rates of displacements and velocities equal their time derivatives and

equilibrium is enforced at a priori fixed instants t_β, t_γ and t_δ, respectively. While (*iii*) is not pertinent here, let us apply hypotheses (*i*) and (*ii*) to the PWL IM, Eq.21, thus obtaining the following LCP in finite increments:

$$\boldsymbol{\varphi}_n + \rho\Delta\boldsymbol{\varphi}_n = \boldsymbol{\varphi}_n + \rho(\mathbf{N}^T\mathbf{D}\Delta\hat{\mathbf{w}}_n - \mathbf{K}\Delta\boldsymbol{\lambda}_n) \leq \mathbf{0},$$

$$\Delta\boldsymbol{\lambda}_n \geq \mathbf{0}, \quad (\boldsymbol{\varphi}_n + \rho\Delta\boldsymbol{\varphi}_n)^T\Delta\boldsymbol{\lambda}_n = 0 \tag{44}$$

The above formulation for $\rho = 1$, i.e. specialised to the backward difference scheme, is seen to coincide with the stepwise holonomic formulation Eqs.39 and 40. The further "no new yielding" hypothesis leading to formulation 43, see preceding remark (b), makes the midpoint instant ρ immaterial.

(d) Of course, the above circumstances noted at (a)–(c) are consequences of the PWL approximation which makes the gradients in Eqs.1, 3 and 4 independent from ρ (and constant). It is worth remembering that the backward difference scheme is often adopted in view of its computationally favourable properties: in particular, algorithmic stability (in the sense of contractivity of disturbances along the step sequence), which turns out to be unconditional for stable laws, conditional (i.e. for Δt_n below a suitable threshold) in the presence of material instability (see e.g. Comi, Corigliano and Maier (1992)).

(e) Damage has been ruled out herein by hypothesis. However, elastic-plastic-damage PWL IMs can easily be dealt with through the very same time-stepping procedures of Subsections 3.1 and 3.2 by preserving the centrality of the LCP format. In fact, the elastic stiffness matrix $\mathbf{D}$ can be updated at the beginning of each step on the basis of the internal variables $\boldsymbol{\lambda}_n$, when the dependence $\mathbf{D}(\boldsymbol{\lambda}_n)$ is provided by experiments and suitable idealisation. Of course, thus an approximation is introduced into the time-integration technique of Subsection 3.1, which, hence, is no longer "exact".

3.4 Holonomic modes

Consider now a single step of the input displacement discontinuity from the origin of its reference frame (namely: $\boldsymbol{\varphi}_n = \mathbf{0}$, $\hat{\mathbf{w}}_n = \mathbf{0}$, $\boldsymbol{\lambda}_n = \mathbf{0}$). Then, Eqs.39–41 give rise to the fully holonomic model in its inverse ($\mathbf{w} \rightarrow \mathbf{p}$) formulation:

$$\begin{gathered}\boldsymbol{\varphi} = \mathbf{N}^T\mathbf{D}\mathbf{w} - \mathbf{K}\boldsymbol{\lambda} - \mathbf{Y} \leq \mathbf{0}, \qquad \boldsymbol{\lambda} \geq \mathbf{0}, \\ \boldsymbol{\varphi}^T\boldsymbol{\lambda} = 0, \qquad \mathbf{p} = \mathbf{D}\mathbf{W} - \mathbf{D}\mathbf{V}\boldsymbol{\lambda}\end{gathered} \tag{45}$$

The direct ($\mathbf{p} \rightarrow \mathbf{w}$) holonomic formulation reads:

$$\begin{gathered}\boldsymbol{\varphi} = \mathbf{N}^T\mathbf{p} - \mathbf{H}\boldsymbol{\lambda} - \mathbf{Y} \leq \mathbf{0}, \qquad \boldsymbol{\lambda} \geq \mathbf{0}, \\ \boldsymbol{\varphi}^T\boldsymbol{\lambda} = 0, \qquad \mathbf{w} = \mathbf{D}^{-1}\mathbf{p} + \mathbf{V}\boldsymbol{\lambda}\end{gathered} \tag{46}$$

Holonomic means here independent of the response from the input history, like in (nonlinear) elasticity and in classical "deformation theory" of plasticity. A prototype of holonomic PWL IM is represented by frictionless unilateral contact in Signorini-Fichera problems. As a specialisation of Eq.45 for N = V = 1, it reads:

$$\varphi = Dw - (D+H)\lambda - Y + Dw_0 \leq 0, \qquad \lambda \geq 0, \quad (47a)$$

$$\varphi\lambda = 0, \qquad p = D(w - \lambda + w_0) \qquad (47b)$$

Here w_0 (≥ 0) represents the pre-existing gap and $Y = 0$, $D \rightarrow \infty$, $H \rightarrow 0$. By these further specialisations, the direct IM (p as input) is arrived at in its traditional formulation:

$$\varphi = p \leq 0, \qquad \lambda = w + w_0 \geq 0, \qquad p\lambda = 0 \tag{48}$$

It is worth noting that also elastic-locking behaviours can be modelled as special cases of holonomic PWL IM. Such models are practically useful in analysis and design of structures containing slackening elements (e.g. cables in tension, semi-rigid joints), but will not explicitly considered herein.

Clearly, in a variety of engineering situations, both dissipative (non-holonomic, irreversible) and reversible (holonomic) behaviours must be considered simultaneously in order to realistically model the same interface, e.g. when loss of contact (and, hence, holonomy) intervenes after frictional contact. Such transitions are easily accounted for at the beginning of each step while formulating the LCP to solve, both in the "exact" (Subsection 3.1) and in the stepwise holonomic procedure (Subsection 3.2).

4 Special cases of mixed-mode piecewise linear models

4.1 Models for joints

As a first example, we consider a simple PWL model apt to describe the essential features of the nonlinear mechanical behaviour of an interface such as a joint in a gravity dam, in view of quasi-static overall analysis of it. A two-dimensional holonomic interpretation of the considered PWL IM is visualised in Figs. 2 and 3 according to the direct ($\mathbf{p} \rightarrow \mathbf{w}$) formulation Eq.46 with no elasticity ($\mathbf{D}^{-1} = \mathbf{0}$).

Three yield loci (yield "planes" or modes) show up in the $\mathbf{p}^T = \{p_n,\ p_t\}$ plane of Fig. 2a.

The locus $\varphi_1 = 0$ prevents tensile tractions, does not move and is associative: only a detachment ($w_n > 0$) can be generated, independently from the value of the shear traction. Clearly, this unilateral contact mode I ($r = 1$) can be expressed in the form 48 with $w_0 = 0$ and subscript 1. For compressive traction ($p_n < 0$), the yield shear traction p_t increases linearly with $|p_n|$, according to the friction parameter μ like in classical Coulomb model. The yield shear traction p_t gives rise to relative displacement along direction $\mathbf{V}_2$ or $\mathbf{V}_3$, generally deviated from the outward normal $\mathbf{N}_2$ or $\mathbf{N}_3$ in order to avoid excessive dilatancy. Since the smoothing of the asperities reduces cohesion (to zero for $p_n = 0$), the loci $\varphi_2 = 0$ and $\varphi_3 = 0$ move inward at yielding of either of them, i.e. they exhibit softening and interaction. Therefore, the residual shear strength (and cohesion) c should depend on the plastic multipliers (and internal variables) λ_r gathered in vector $\boldsymbol{\lambda}$:

$$\varphi_2 = p_t + \mu p_n - c(\boldsymbol{\lambda}) \leq 0,\ \lambda_2 \geq 0,\ \varphi_2\lambda_2 = 0 \qquad (49a)$$

$$\varphi_3 = -p_t + \mu p_n - c(\boldsymbol{\lambda}) \leq 0,\ \lambda_3 \geq 0,\ \varphi_3\lambda_3 = 0 \qquad (49b)$$

Clearly, the translation of the above yield loci 2 and 3 stops at the loci shown by dashed lines in Fig. 2, since afterwards a truly Coulombian behaviour is assumed, as visualised in Fig. 3. In order to account for this fact in the PWL model, a fourth internal variable λ_4 is introduced and the dependence $c(\boldsymbol{\lambda})$ is assumed linear as follows:

$$c(\boldsymbol{\lambda}) = c_0 + H_t(a\lambda_1 + \lambda_2 + \lambda_3 - \lambda_4) \equiv -\varphi_4 \geq 0, \qquad (50a)$$

$$\lambda_4 \geq 0, \qquad \varphi_4\lambda_4 = 0 \qquad (50b)$$

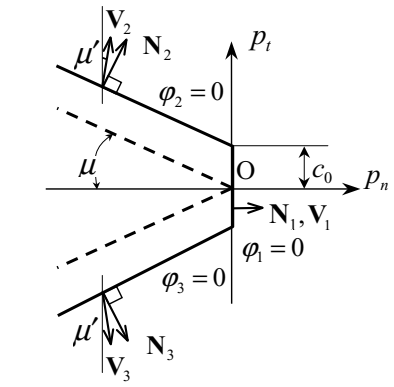

(a)

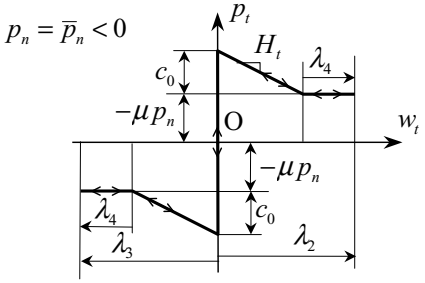

(b)

Figure 2 : Simple two-dimensional PWL frictional model for a joint with cohesion c_0: (a) yield modes in the traction plane; (b) specialization to a case with assigned compressive normal traction ($p_n < 0$).

The idealised behaviour, visualised in Fig. 2, can be mathematically described by the following relations:

$$\begin{Bmatrix} \varphi_1 \\ \varphi_2 \\ \varphi_3 \\ \varphi_4 \end{Bmatrix} = \begin{bmatrix} 1 & 0 \\ \mu & 1 \\ \mu & -1 \\ 0 & 0 \end{bmatrix} \begin{Bmatrix} p_n \\ p_t \end{Bmatrix} - H_t \begin{bmatrix} 0 & 0 & 0 & 0 \\ a & 1 & 1 & -1 \\ a & 1 & 1 & -1 \\ a & 1 & 1 & -1 \end{bmatrix} \begin{Bmatrix} \lambda_1 \\ \lambda_2 \\ \lambda_3 \\ \lambda_4 \end{Bmatrix} - \begin{Bmatrix} 0 \\ c_0 \\ c_0 \\ c_0 \end{Bmatrix} \qquad (51)$$

$$\varphi_r \leq 0, \quad \lambda_r \geq 0, \quad \varphi_r\lambda_r = 0 \quad (r = 1, \ldots, 4) \qquad (52)$$

$$\begin{Bmatrix} w_n \\ w_t \end{Bmatrix} = \begin{bmatrix} 1 & u' & u' & 0 \\ 0 & 1 & -1 & 0 \end{bmatrix} \begin{Bmatrix} \lambda_1 \\ \vdots \\ \lambda_4 \end{Bmatrix} \qquad (53)$$

where parameter H_t (≤ 0) can be interpreted as a softening modulus and the coupling parameter a quantifies the cohesion reduction due to the detachment mode I measured by λ_1.

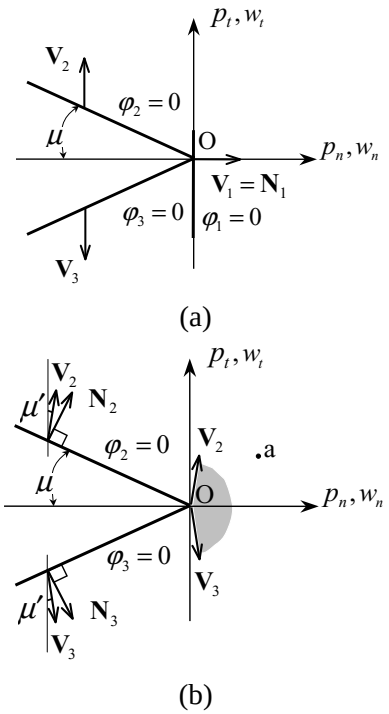

Figure 3 : Specialization of the model of Figure 2 to Coulomb friction models without dilatancy (a) and with dilatancy (b).

The internal variable λ_4 has been introduced in order to stop the aforementioned translation when the cohesion c vanishes. In fact, it neutralises the effects of the others (λ_1, λ_2, λ_3) when and only when $c = 0$, if c is interpreted as a fourth yield function ($\varphi_4 \equiv -c$) related by complementarity to λ_4, as expressed in Eq.50. It is worth noting that the fourth yield mode does not involve tractions and, hence, cannot be represented in the traction space of Fig. 2a (this "hidden mode" might be visualised in the "augumented (hyper) space" of all variables: tractions p_n and p_t and internal variables λ_r).

In the light of the above considerations, Eqs.51–52 represent a LCP with a nonsymmetric indefinite matrix, and Eqs.51–53 can be regarded as a special case (with $n_y = 4$) of Eq.46.

Consider now, as specialisation of the above PWL model, the classical Coulomb friction model with no dilatancy, Fig. 3a, and with dilatancy attenuated through nonassociativity ($\mu' < \mu$), Fig. 3b. In both cases one has to set $H_t = 0$ in Eq.51 (which thus no longer involves plastic multipliers λ_r) and to remove from Eq.51 the "hidden" 4-th yield mode $\varphi_4 = 0$. In the latter case, with $\mu' > 0$, displacement w_n can be generated at the origin $\mathbf{p} = \mathbf{0}$ by linear combinations of the unit vectors $\mathbf{V}_2$, $\mathbf{V}_3$ projected on axis w_n ($w_n = \lambda_2\, V_{2n} + \lambda_3\, V_{3n}$). Therefore, yield mode $r = 1$ is not needed and, hence, $w_n = \mu'(\lambda_2 + \lambda_3)$ from Eq.53: thus, consistently with an idealised physical links between dilatancy and asperities, the set of displacement jumps correponding to $\mathbf{p} = \mathbf{0}$ is confined to the angle between $\mathbf{V}_2$ and $\mathbf{V}_3$ centered in the origin $\mathbf{O}$, as shown in Fig. 3b. In Coulomb's simplest special case, after the above specialisations, the $\mathbf{w} \rightarrow \mathbf{p}$ relationship, inverse to Eqs.51–53, reads:

$$\left\{ \begin{array}{c} \varphi_2 \\ \varphi_3 \end{array} \right\} = \left[\begin{array}{cc} \mu D_n & D_t \\ \mu D_n & -D_t \end{array} \right] \left\{ \begin{array}{c} w_n \\ w_t \end{array} \right\} + - \left[\begin{array}{cc} \mu\mu' D_n + D_t & \mu\mu' D_n - D_t \\ \mu\mu' D_n - D_t & \mu\mu' D_n + D_t \end{array} \right] \left\{ \begin{array}{c} \lambda_2 \\ \lambda_3 \end{array} \right\} \tag{54}$$

$$\varphi_r \leq 0, \qquad \lambda_r \geq 0, \qquad \varphi_r \lambda_r = 0 \quad (r = 2,3) \tag{55}$$

$$\left\{ \begin{array}{c} p_n \\ p_t \end{array} \right\} = \left[\begin{array}{cc} D_n & 0 \\ 0 & D_t \end{array} \right] \left\{ \begin{array}{c} w_n \\ w_t \end{array} \right\} - \left[\begin{array}{cc} \mu' D_n & \mu' D_n \\ D_t & -D_t \end{array} \right] \left\{ \begin{array}{c} \lambda_2 \\ \lambda_3 \end{array} \right\} \tag{56}$$

It is worth noting that the LCP in Eqs.54−55 has a symmetric positive-definite matrix and, therefore, its solution $\boldsymbol{\lambda}$ is unique (see e.g., Cottle, Pang and Stone (1992)). It is readily seen that $\mathbf{p} = \mathbf{0}$ corresponds to any displacement jump $\mathbf{w}$ belonging to the open angle $\mathbf{V}_2\hat{\mathbf{O}}\mathbf{V}_3$, like point **a** in Fig. 3b. In the former, no-dilatancy case of Fig. 3a, the yield mode $\varphi_1 = 0$ is preserved in Eqs.51–53 and all points in both quadrants $w_n > 0$ correspond to $\mathbf{p} = \mathbf{0}$.

The possible presence of an initial gap $w_{0n} > 0$ in the joint can be accounted for simply by replacing w_n by $w_n + w_{0n}$ in the preceding models.

In some nonlinear IMs proposed in the literature (e.g. Carol, Prat and Lopez (1997), Lotfi and Shing (1994)) the dilatancy decreases for increasing compressive normal traction. This feature can easily be accomodated in the present PWL category of IMs by adding two (or more) yielding modes as shown in Fig. 4. The relevant LCP description, which extends Eqs.51–53, reads:

$$\left\{\begin{array}{c}\varphi_1\\ \varphi_2\\ \varphi_3\\ \varphi_4\\ \varphi_5\\ \varphi_6\end{array}\right\}=\left[\begin{array}{cc}1 & 0\\ \mu & 1\\ \mu & -1\\ 0 & 1\\ 0 & -1\\ 0 & 0\end{array}\right]\left\{\begin{array}{c}p_n\\ p_t\end{array}\right\}+ \tag{57}$$

$$-H_t\left[\begin{array}{cccccc}0&0&0&0&0&0\\ a&1&1&1&1&-1\\ a&1&1&1&1&-1\\ a&1&1&1&1&-1\\ a&1&1&1&1&-1\\ a&1&1&1&1&-1\end{array}\right]\left\{\begin{array}{c}\lambda_1\\ \lambda_2\\ \lambda_3\\ \lambda_4\\ \lambda_5\\ \lambda_6\end{array}\right\}-\left\{\begin{array}{c}0\\ c_0\\ c_0\\ c_0+\Delta c\\ c_0+\Delta c\\ c_0\end{array}\right\}$$

$$\varphi_r\le 0,\qquad \lambda_r\ge 0,\qquad \varphi_r\lambda_r=0\quad (r=1,\ldots,6) \tag{58}$$

$$\left\{\begin{array}{c}w_n\\ w_t\end{array}\right\}=\left[\begin{array}{cccccc}1&\mu'&\mu'&0&0&0\\ 0&1&-1&1&-1&0\end{array}\right]\left\{\begin{array}{c}\lambda_1\\ \vdots\\ \lambda_6\end{array}\right\} \tag{59}$$

It is worth noting that the 6-th yield mode ($\varphi_6 = 0$) is "hidden" like the 4-th in the preceding model (Fig. 2): in fact, it cannot be represented in the traction plane, but acts here as arrestor of the shrinking motion of modes 2, 3, 4, and 5 due to softening (Fig. 4).

There are six material parameters in this model: the softening modulus H_t; the original cohesion c_0 (original shear strength); the shear strength growth Δc due to high compression; the friction coefficient μ; the deviation from normality $\mu-\mu'$, intended to reduce dilatancy; the coefficient a which quantifies the interaction of yield mode 1 with the others.

4.2 A cohesive crack model

Then a quasi-brittle fracture process has to be described by a PWL model, adhesion must be allowed for, consistently with the popular cohesive crack p_n versus w_n relation for mode I visualised in Fig. 1a. To this purpose, the PWL model of Fig. 4 is adjusted as shown in Fig. 5 by conferring tensile strength χ_0, i.e. merely translating outward the yield mode $\varphi_1 = 0$. Clearly, this yield locus is characterised by a softening modulus $H_n < 0$ and, hence, at yielding it translates inwards up to the origin **O**. When the origin is reached, this translation stops by the activation of another mode, i.e. the seventh one. The role of this mode ($\varphi_7 = 0$) is similar to that of the 6-th one in the model of Fig. 4, namely it does not involve the tractions (and hence, can not be represented in Fig. 5), but it linearly involves the plastic multipliers $\lambda_1 \ldots \lambda_5$, of all the 5 yield modes visible in Fig. 5 and λ_7: in the framework of the yield mode interaction, this 7-th mode stops the softening re-entrant motion of the yield mode 1.

Mathematically, the mixed mode PWL cohesive crack model in point is represented by the following generalisation of Eqs.57–58:

$$\left\{\begin{array}{c}\varphi_1\\ \varphi_2\\ \varphi_3\\ \varphi_4\\ \varphi_5\\ \varphi_6\\ \varphi_7\end{array}\right\}=\left[\begin{array}{cc}1 & 0\\ \mu & 1\\ \mu & -1\\ 0 & 1\\ 0 & -1\\ 0 & 0\\ 0 & 0\end{array}\right]\left\{\begin{array}{c}p_n\\ p_t\end{array}\right\}-\left\{\begin{array}{c}\chi_0\\ c_0\\ c_0\\ c_0+\Delta c\\ c_0+\Delta c\\ c_0\\ \chi_0\end{array}\right\}+ \tag{60}$$

$$-\left[\begin{array}{ccccccc}H_n&bH_n&bH_n&bH_n&bH_n&0&-H_n\\ aH_t&H_t&H_t&H_t&H_t&-H_t&0\\ aH_t&H_t&H_t&H_t&H_t&-H_t&0\\ aH_t&H_t&H_t&H_t&H_t&-H_t&0\\ aH_t&H_t&H_t&H_t&H_t&-H_t&0\\ aH_t&H_t&H_t&H_t&H_t&-H_t&0\\ H_n&bH_n&bH_n&bH_n&bH_n&0&-H_n\end{array}\right]\left\{\begin{array}{c}\lambda_1\\ \lambda_2\\ \lambda_3\\ \lambda_4\\ \lambda_5\\ \lambda_6\\ \lambda_7\end{array}\right\}$$

$$\varphi_r\le 0,\qquad \lambda_r\ge 0\qquad \varphi_r\lambda_r=0\quad (r=1,\ldots,7) \tag{61}$$

$$\left\{\begin{array}{c}w_n\\ w_t\end{array}\right\}=\left[\begin{array}{ccccccc}1&\mu'&\mu'&0&0&0&0\\ 0&1&-1&1&-1&0&0\end{array}\right]\left\{\begin{array}{c}\lambda_1\\ \vdots\\ \lambda_7\end{array}\right\}+\mathbf{D}^{-1}\left\{\begin{array}{c}p_n\\ p_t\end{array}\right\} \tag{62}$$

Besides possible elastic stiffnesses in matrix **D** (assumed as diagonal), the material parameters to identify on the basis of experimental data are now: H_n, H_t, c_0, Δc, χ_0, μ, μ', a, b. Their meanings partly emerge from Eq.60 and partly are specified in Fig. 5.

5 Numerical tests

This Section is intended to investigate and illustrate the behaviour and the representation capacity of the PWL interface models formulated and discussed in general terms in Section 2, and specialised to some representative cases in Section 4. The algorithm employed for the numerical solution of the LCPs arising in the tests which follow, is outlined in Section 6.

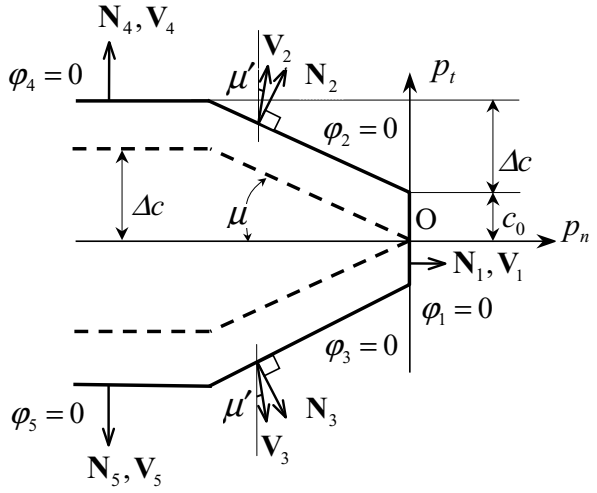

Figure 4 : Improvement of the interface model of Figure 2 by the elimination of unrealistic dilatancy through additional yield modes, see Eqs.57-59.

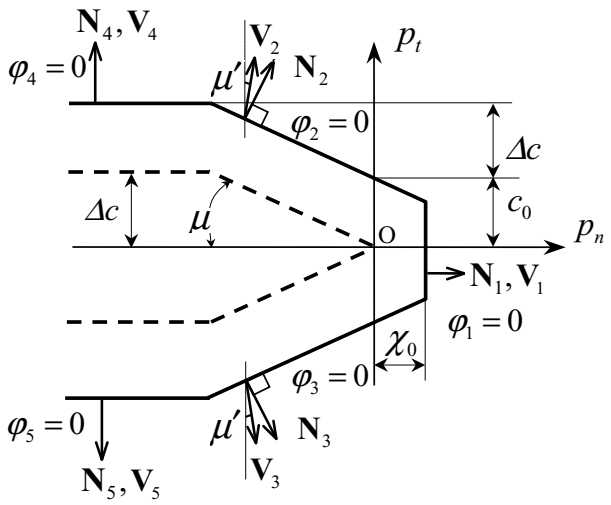

Figure 5 : Piecewise linear cohesive crack model for mixed-mode quasi-brittle fracture, see Eqs.60-62, as an extension (by conferral of tensile strength) of the model of Figure 4.

5.1 A joint model

First, consider the interface model depicted in Fig. 4 in its holonomic formulation described by Eqs.51-53 and quantified here by assigning the following values to the available parameters (in accordance with data in Ahmadi, Izadinia and Bachmann (2001)): softening modulus H_t=–2 MPa ·mm^{-1}; cohesion c_0=4.0 MPa; Δc=14 MPa; friction coefficient $\mu = 0.7$; dilatancy $\mu' = 0.364$; interaction coefficient $a = 0.8$; elastic stiffness D_n=40 MPa ·mm^{-1}, D_t = 20 MPa ·mm^{-1} without interaction.

Figure 6 provides checks of, and insight into, the direct relationship $\mathbf{p} \rightarrow \mathbf{w}$, namely: two **p**-paths, (a,b,c,b,a) and (a',b',c',d',e',d',c',b',a') are assumed as input and are indicated in Fig. 6a, where the quantified yield modes are also represented. In Fig. 6b points mark the holonomic responses, i.e. vectors **w** computed for the input data **p** with the same symbols; the graph (c) shows the non-holonomic responses computed exactly (cp. Section 3) for the two paths now conceived as cyclic starting from the origin **a** and going back to it. In Figs. 7a-c the inverse relationship $\mathbf{w} \rightarrow \mathbf{p}$ is dealt with, like the direct one in Figs. 6a-c.

The numerical exercises illustrated in Figs. 6 and 7 give rise to the comments which follow.

(*i*) Consider first the sequence of points **a**, **b**, **c** (i.e. of vectors $\mathbf{p}_a$, $\mathbf{p}_b$, $\mathbf{p}_c$) in Fig. 6a, and the holonomic model.

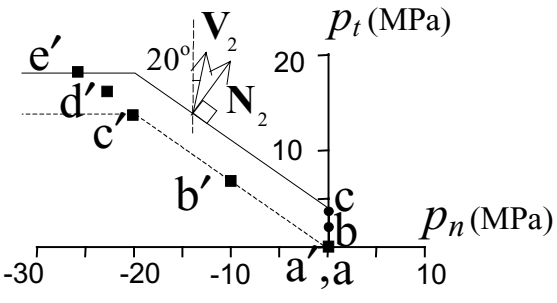

(a)

Figure 6 : Tests on the joint model of Figure 4: (a) two inputs in terms of proportional tractions (a,b,c,b,a) and (a',b',c',d',e',d',c',b',a');

With the input $\mathbf{p}_a = \mathbf{0}$, the LCP formulated by Eqs.51 and 52, through the solution by the enumerative algorithm of Section 6, leads to output vectors $\mathbf{w}_{a1}$ and $\mathbf{w}_{a2}$, i.e. to points $\mathbf{a}_1$ and $\mathbf{a}_2$ in Fig. 6b. These are singular points for the infinite set of displacements **w** corresponding to $\mathbf{p}_a = \mathbf{0}$. Mathematically, this set is related to the singularity of matrix **H** (of order 4 and rank 1). Mechanically, the set can be singled out as follows: since $\lambda_1 > 0$ and, hence, the detachment $w_n > 0$ grows, the shear strength decreases and this decohesion is reflected in the model by the interaction of yield mode 1 on yield mode 2 and 3. The cohesion vanishes when $w_n = \lambda_1 = 2.5$, i.e. in point $\bar{\mathbf{a}}_1$; then any combination of opening and sliding

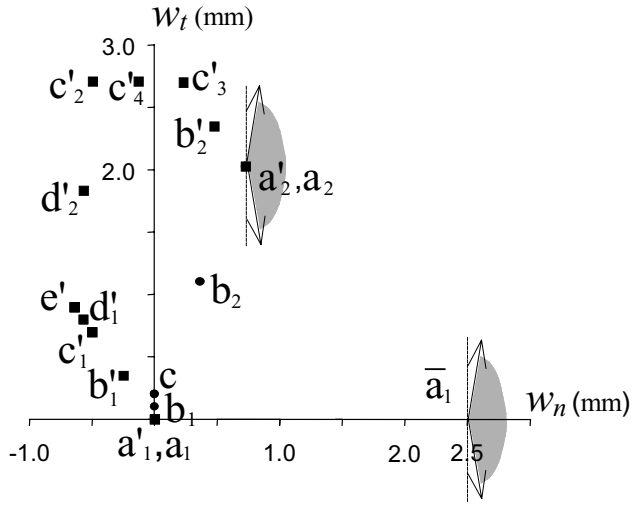

(b)

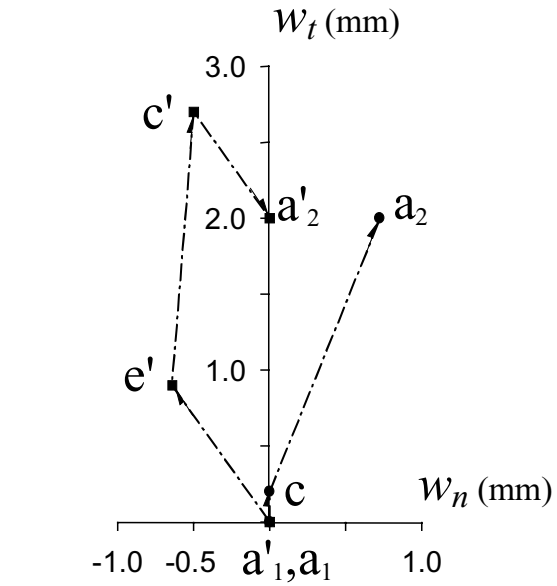

(c)

Figure 6 : (Continued) (b) displacement discontinuities corresponding to the tractions marked in (a) through the model Eqs.51-53 in the holonomic version; (c) paths of relative displacements corresponding to the traction paths assumed in (a) obtained with the non-holonomic model, Eqs.18-19.

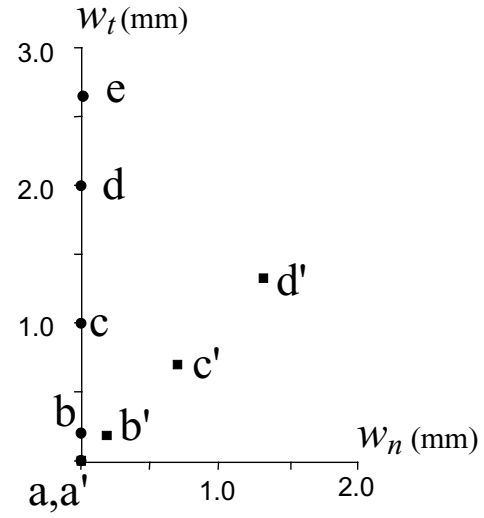

(a)

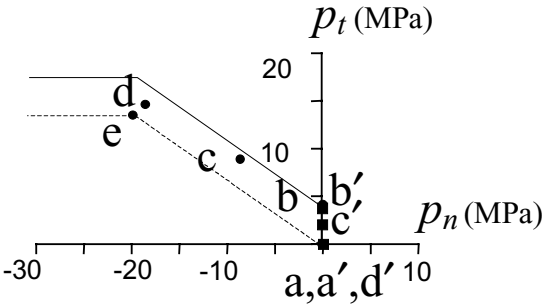

(b)

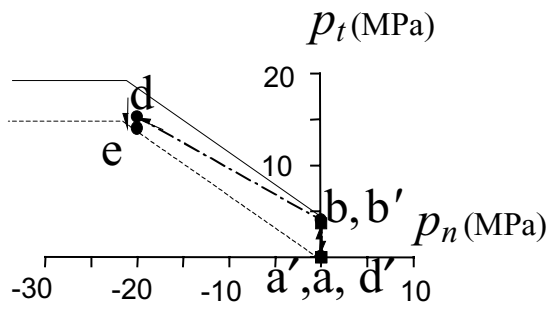

(c)

Figure 7 : Same meaning of the graphs as in Figure 6, but using the inverse relationship $\mathbf{w} \rightarrow \mathbf{p}$.

displacements in the fan shown in Fig. 6b corresponds to $\mathbf{p}_a = \mathbf{0}$, the fan being defined by vectors $\mathbf{V}_2$ and $\mathbf{V}_3$. The numerical solution of LCP, Eqs.51–52, for $\mathbf{p}_a = \mathbf{0}$ provides, besides $\mathbf{w}_{a1}$, also vector $\mathbf{w}_{a2}$ (point $\mathbf{a}_2$ in Fig. 6b). In fact, the origin **a** of the **p**-plane can be attained after the loop (**a**, **c**, **a**) with activation in **c** of only yield mode $\varphi_2 = 0$; this model "softens" along the return of **p** to the origin, thus generating at the end the displacement $\mathbf{w}_{a2}$ marked by $\mathbf{a}_2$ in Fig. 6b. Thereafter, any further displacement may occur with $\mathbf{p} = \mathbf{0}$ within the fan $\mathbf{V}_2 \hat{a}_2 \mathbf{V}_3$ centered in $\mathbf{a}_2$, as visualised in Fig. 6b. Contrary to the multiplicity of solution for $\mathbf{p}_a = \mathbf{0}$, a unique holonomic response $\mathbf{w}_c$ is noticed to correspond to $\mathbf{p}_c$ at the vertex of the yield domain (Fig. 6a).

(*ii*) A path of reasoning similar to the preceding one and not presented herein for brevity, may lead to similar mechanical interpretations of the multiple solutions to the LCP, Eqs.51–52, indicated in Fig. 6b with numbering subscript (e.g. $\mathbf{c'}_1, \ldots \mathbf{c'}_4$), for various inputs (e.g. point **c'**) specified in Fig. 6a.

(*iii*) Let us focus now on the present PWL IM in its non-holonomic version according to Eqs.18–19. Exact integration in the sense of Subsection 3.1 leads from the two input paths shown in Fig. 6a to the output paths depicted in Fig. 6c. Point **b** is automatically skipped in the exact integration because no new yield mode is activated in it. Multiplicity of solutions is noticed to be drastically reduced, as expected from the irreversibility of the model.

Figure 7 is intended to illustrate the relationship $\mathbf{w} \rightarrow \mathbf{p}$ inverse to Eqs.51–53, i.e. to the joint PWL IM qualitatively depicted in Fig. 4. The **w**-input considered, the computed tractions $\mathbf{p}_a$, $\mathbf{p}_b$ ... corresponding to $\mathbf{w}_a$, $\mathbf{w}_b$ ... through the holonomic model and the non-holonomic response paths computed by the "exact" integration of Subsection 3.1, are specified in Figs. 7a, b, c, respectively. The main general feature to be observed in these pictures is the uniqueness of the holonomic output, in contrast to what was noticed, see remark (*i*), for the direct holonomic output of Fig. 6b. Clearly, this ("stabilising") effect of the inversion, well expected in mechanical terms, mathematically is a consequence of the rank increase in passing, in the LCP to solve, from matrix **H** to matrix **K**, Eq.23, through the addition of the elastic stiffness **D**. In fact, the 4-th order matrix **K** in the present case is of rank 3 (though still nonsymmetric and nondefinite).

5.2 A cohesive crack model

Focus is now on the mixed-mode cohesive crack model with 7 yield modes, described by Eqs.60–62 and visualised in Fig. 5. The nine material parameters, defined in Subsection 4.2, are given the following values (selected in accordance with data in Carol, Prat and Lopez (1997)): $H_n = -60$ MPa $\cdot$ mm^{-1}; $H_t = -28$ MPa $\cdot$ mm^{-1}; $\Delta c = 20$ MPa; $c_0 = 7.0$ MPa; $\chi_0 = 3$ MPa; $\mu = 0.9$; $\mu' = 0.364$; $a = 0.8$; $b = 0.2$. Like in Subsection 5.1, the elastic stiffness matrix is regarded as diagonal with $D_n = D_t = 200$ MPa $\cdot$ mm^{-1}. Several numerical tests are presented in Figs. 8 and 9 and give rise to the following remarks.

(*i*) As specified in Subsection 4.2, the novelties with respect to the joint model of Fig. 4 discussed in what precedes, are as follows: the yield mode $\varphi_1 = 0$ is now endowed with tensile strength χ_0 and softening; the softening yield modes 4 and 5 are added in order to reduce the influence of significant compression p_n on shear strength. Otherwise the essential features are the same, a circumstance which shortens the present discussion.

(*ii*) The model is assumed as holonomic when irreversibility manifestations are ruled out by hypothesis, since proportional traction paths are considered as input, like the two indicated in Fig. 8a: (**a**, **b**, **c**, **d**) and (**a**', **b**', **c**'). Like in Subsection 5.1, the questions are: which displacement vectors $\{w_n, w_t\} = \mathbf{w}^T$ correspond, through the model, to a given traction vector $\{p_n, p_t\} = \mathbf{p}^T$; inversely, which **p** to given **w**. Answers are achieved by solving the LCP Eqs.60–61. They are visualised in Figs. 8b, c and 9b, respectively. Paying special attention to solution multiplicity, the set of displacement jumps corresponding to $\mathbf{p}_a = \mathbf{0}$ is analogous to that in Fig. 6b, but only the fan centered in $\mathbf{a'}_3$ is visualised in Fig. 8b, since the counterpart $\overline{a}_1\,(0.31,\, 0)$ to point $\overline{a}_1$ in Fig. 6b is too far from the reference origin. In view of the similarity with the remark (*i*) in Subsection 5.1, a detailed discussion is omitted.

(*iii*) The non-holonomic version of the direct and inverse multidissipative PWL IM in point and the interpretation of the primed and unprimed sequences of data (Figs. 8a and 9a) as assigned closed-loop paths (a $\rightarrow$a), lead to the response paths which are visualised in Figs. 8d and 9c, respectively: they were computed by the "exact" integration procedure described in Subsection 3.1, using once again, at every new yield mode activation, the LCP algorithm outlined in the next Section.

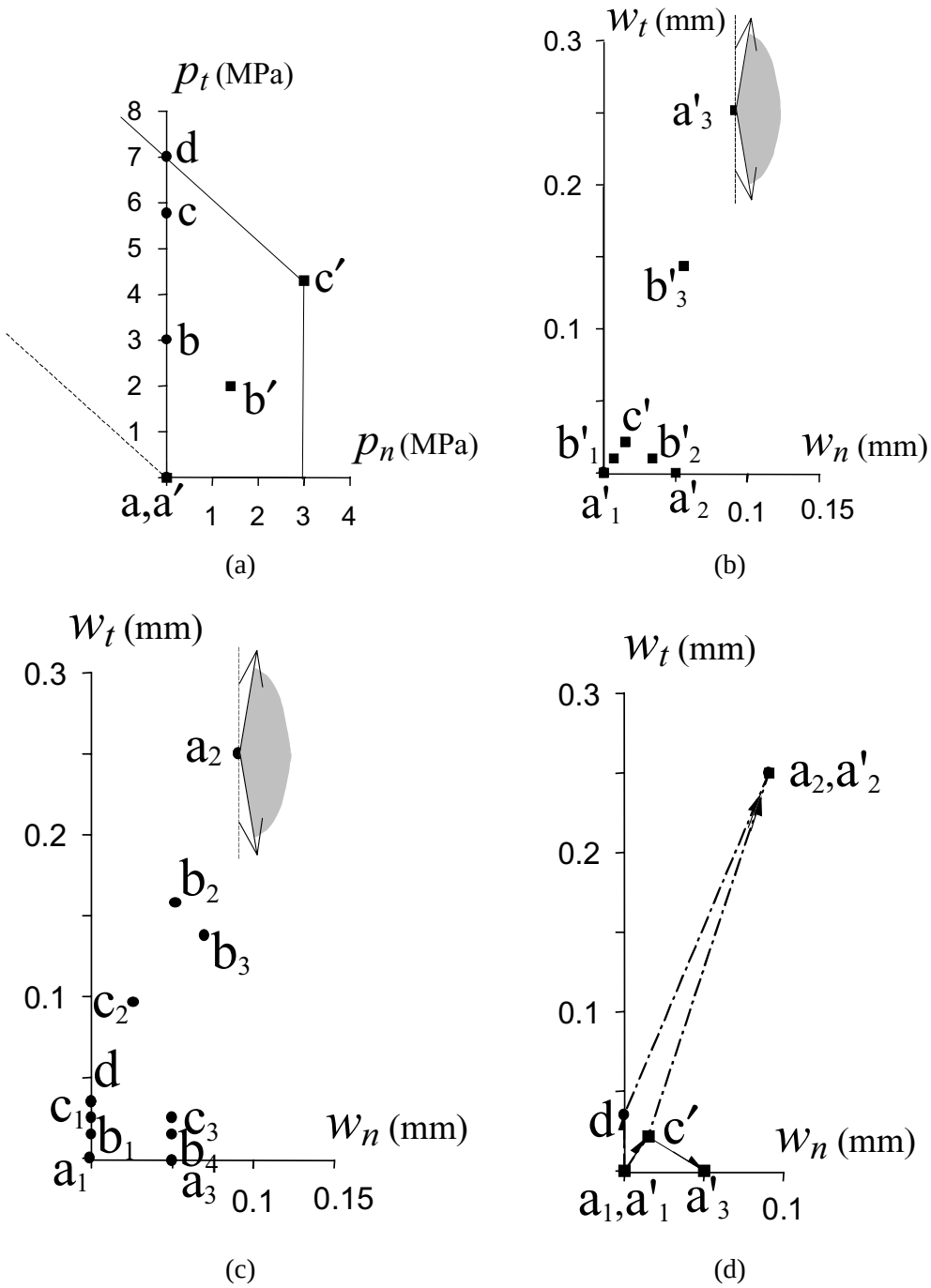

Figure 8 : Tests on the cohesive model of Figure 5: (a) given proportional traction sequences (a,b,c,d,c,b,a) and (a',b',c',b',a'); (b) and (c) relative displacement corresponding to the tractions marked in (a) through the holonomic version of the model; (d) paths of relative displacements as nonholonomic responses to the traction paths visualized in (a).

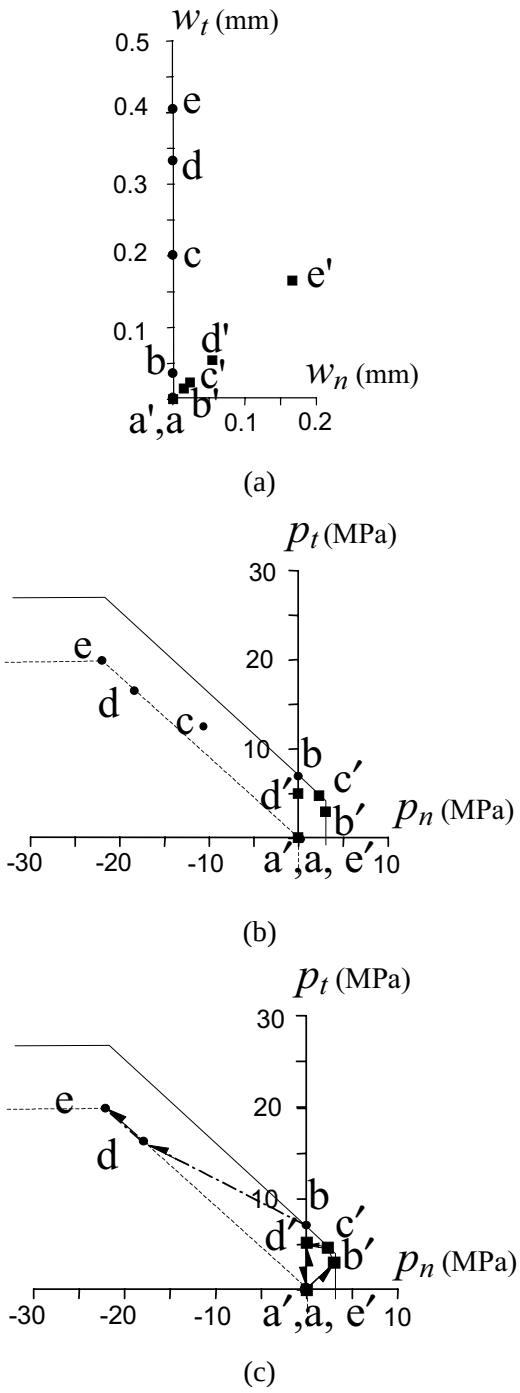

Figure 9 : Same meaning of the graphs like in Figure 8, but using the inverse relationship $\mathbf{w} \rightarrow \mathbf{p}$.

6 On algorithms for linear complementarity problems

From the computational standpoint, a recurrent pivotal role, in what precedes, is played by linear complementarity problems (LCPs). In order to clarify some peculiar features of this special mathematical construct and of its solution algorithms, consider e.g. the LCP involved in the direct ($\mathbf{p} \rightarrow \mathbf{w}$) holonomic PWL model Eq.46. Setting $\mathbf{d} \equiv \mathbf{Y} - \mathbf{N}^T\,\mathbf{p}$ (vector of data), that LCP reads:

$$-\boldsymbol{\varphi} = \mathbf{H}\boldsymbol{\lambda} + \mathbf{d} \geq \mathbf{0}, \qquad \boldsymbol{\lambda} \geq \mathbf{0}, \qquad \boldsymbol{\varphi}^T\boldsymbol{\lambda} = 0 \tag{63}$$

The treatise of Cottle, Pang and Stone (1992) provides a comprehensive conspectus of the abundant knowledge accumulated up to decade ago on LCP like Eq.63 in terms of theorems on solution existence and multiplicity and of (iterative and pivoting) methods for numerical solutions, mostly related to special properties of matrix **H**. In the present context, the already noted essential features of the LCP problems are: small number of variables (since local, constitutive relationship are considered); general (indefinite, nonsymmetric) matrices **H**, due to softening, nonassociativity and mode interactions (in contrast to traditional elastoplasticity with stability in Drucker's sense); multiplicity of solutions, frequently expected, especially for holonomic PWL models.

These peculiar features led to the adoption, for all the computations, of the "enumerative" method developed by Judice and Mitra (1988). It is briefly outlined below.

Consider the sequence of pairs (φ_r, λ_r) for r = 1 ... n; for n = 1, consider the alternatives $\varphi_1 = 0$ and $\lambda_1 = 0$; if n = 2, there are two other pairs of alternatives; in this way for any n_y a binary tree is generated where each "node" can branch into either $\varphi_r = 0$ or $\lambda_r = 0$, a tree with 2^{n-1} nodes at each level (2^n–1 all together) with n equal to the number n_y of yield planes. In principle, all solutions of a LCP can be found by exploring all the nodes. The enumerative method is based on a strategy which leads along all the n_y levels of the above tree to the LCP solutions: each move from one node to a neighbouring one entails the solution of a linear programming problem (LPP) (precisely, the linearly constrained minimisation of a λ_n one branch and a $-\varphi$ on the other). Each LPP solution provides guidance for skipping some descending branch ("pruning") and criteria for nonexistence of LCP solutions and for singling out all solutions

when level n_y is reached. The process is initialised at a vertex of the hyperpolyhedron defined in the $\boldsymbol{\lambda}$-space by the linear inequalities in Eq.63. This vertex or "basic feasible vector" (which represents the first node of the binary tree) is computed by LP, like in "phase one" of the classical Simplex method.

The sketchy outline which precedes corroborates the following peculiarities of the enumerative algorithm adopted: (*i*) all meaningful solutions of the LCP are captured (or evidence given that none exists) after a finite sequence of LP subproblems solved by some advanced pivotal LP algorithm, therefore with finite termination; by "meaningful" solutions we mean here those which characterise an infinity of other solutions, like point $\mathbf{a}_2$ in Fig. 6b. (*ii*) exponential growth of computing time with problem size in view of the combinatorial nature of the strategy adopted.

Clearly, in the present study of multidissipative constitutive models the pro (*i*) by far prevails on the con (*ii*). For overall structural analysis purposes (dealt with elsewhere) the contrary holds true, and, hence, recourse to other, conceptually different algorithms becomes mandatory, such as a general pathsearch damped Newton method ("Path"), proposed by Dirkse and Ferris (1995) and employed in mode I fracture simulations e.g. by Tin-Loi and Ferris (1997).

7 Conclusions

In this paper a peculiar class of elastic-plastic relationships between tractions and work-conjugate displacements has been studied, in order to provide simple and unified mathematical modelling tools for inelastic analysis of structures where practically important nonlinear dissipative phenomena can be assumed to be localised on loci of displacement discontinuities. As a typical example, in concrete dams these loci may include artificial joints, existing cracks and process zones of quasi-brittle fracture interpreted by cohesive crack "discrete" models.

The peculiarity of the constitutive relationships considered, referred to as interface models (IM), is the "piecewise linearisation" (PWL), i.e. the linearity both of yield functions and of plastic potentials in all the multiple yield modes adopted.

The conclusions achieved herein are as follows.

(a) A single mathematical construct, i.e. the linear complementarity problems (LCP), provides a unifying framework which encompasses: holonomic (path-independent, single step) and non-holonomic (incremental) formulations; direct (from tractions to relative displacements) and inverse relationships; behaviours of joints and fracture processes (obviously, with different selection of yield modes and parameters).

(b) Softening and yield mode interactions imply that the LCPs formulated for PWL IMs are centered on sign-indefinite, generally nonsymmetric matrices, and that often multiplicity or nonexistence of solutions occur, as expected through physical insight.

(c) The above mathematical features require recourse to "ad hoc" algorithms available in the recent literature on mathematical programming. The one employed herein for the numerical tests has been an "enumerative" method capable to compute all solutions (or to prove that none exists). This algorithm was found to be efficient and robust for numerical checks intended to investigate the capacity of the formulated PWL IMs to capture the essential features of the considered relationships between tractions and displacement discontinuities. The enumerative method, because of its combinatorial basis, would not be suitable to overall structural analyses. In fact, structural analysis, which combine PWL IMs and material constitutive models with equilibrium and geometric compatibility, if all nonlinearities are confined to the IMs, preserve the LCP format but, naturally, entail drastic increase of the problem size.

The present subject, and the results achieved herein, require the following further developments: (α) effective procedures for the identification of the model parameters through experimental data or through data provided by more sophisticated nonlinear interface models; (β) assessment of merit in terms of computing cost in large-scale overall analysis of structures, by comparison with other nonlinear IMs; (γ) extensions and applications of PWL IMs to three-dimensional structural analysis.

Acknowledgement: The writers thank Professor F. Tin-Loi for a computer code where the enumerative algorithm was implemented. A MURST grant ("Cofinanziamento 2001") for a research project on "Integrity Assessment of Large Dams" is gratefully acknowledged. Thanks are expressed to Northeastern University, China, for the permission of a leave of absence given to the third author since April 2000.

References

Abraham, F. F. (2000): MAADLY spanning the length scales in dynamic fracture, *CMES:Computer Modeling in Engineering & Sciences*, vol.1, no.4, pp.63-70.

Ahmadi, M.T.; Izadinia, M.; Bachmann, H. (2001): A discrete crack joint model for nonlinear dynamic analysis of concrete arch dam, *Computer and Structures*, vol.79, pp.403-420.

Bolzon, G.; Maier, G.; Tin-Loi, F. (1995): Holonomic and non-holonomic simulation of quasi -brittle fracture: a comparative study of mathematical programming approaches. In: Wittman F. H. (ed.) *Fracture Mechanics of Concrete Structures*, Aedificatio Publishers, Freiburg, pp. 885-898.

Bolzon, G.; Maier G.; Tin–Loi F. (1997): On multiplicity of solutions in quasi–brittle fracture computations, *Computational Mechanics*, vol.19, pp.511–516.

Carini, A.; Maier, G. (2000): Extremum and saddle-point theorems for elastic solids with dissipative displacement discontinuities, *Archives of Mechanics*, vol.52, pp.523-545.

Carol, I.; Prat, P.C.; Lopez, C.M. (1997): Normal/shear cracking model: application to discrete crack analysis, *J. Engng. Mech.*, ASCE, vol.123, pp.1-9.

Cen, Z.; Maier, G. (1992): Bifurcations and instabilities in fracture of cohesive-softening structures: a boundary element analysis, *Fatigue Fract. Engng. Mater. Struct.*, vol.15, pp.911-928.

Comi, C., Corigliano, A., Maier, G. (1992): Dynamic analysis of elastoplastic-softening discretized structures. *Proc. ASCE, J. Eng. Mech.*, vol.118, pp.2352-2375.

Corigliano, A. (1993): Formulation, identification and use of interface models in the numerical analysis of composite delamination. *Int. J. Solids Struct.*, vol.30, pp.2779-2811.

Cottle R. W.; Pang J.S.; Stone R. E. (1992): *The Linear Complementary Problem*, Academic Press, San Diego.

De Donato, O.; Maier, G. (1976): Local unloading in piecewise-linear plasticity, *J. Engng. Mech.*, ASCE, vol.102 (EM3), pp.383-394.

Dirkse, S.P.; Ferris, M.C. (1995): The PATH solver: a non-monotone stabilisation scheme for mixed complementarity problems, *Optimization Methods & Software*, vol.5, pp.123–156.

Fakharian, K.; Evgin, E. (2000): Elasto-plastic modelling of stress-path-dependent behaviour of interfaces. *Int. J. Numer. Analyt. Meth. Geomech.*, vol.24, pp.183-199.

Guinea, G.V.; Planas, J.; Elices, M. (1994): A general bilinear fit for the softening curve of concrete, *Materials and Structures*, vol.27, pp.99–105.

Hassanzadeh, M. (1990): Determination of fracture zone properties in mixed mode I and II, *Engrg. Fracture Mech.*, vol.35, pp.845–853.

Judice, J. J.; Mitra, G. (1988): An enumerative method for the solution of linear complementarity problems, *Eur. J. Operat. Res.*, vol.36, pp.122–128.

Karihaloo, B. L. (1995): *Fracture Mechanics and Structural Concrete*, Longman Scientific & Technical, Harlow, Great Britain.

Lloyd Smith, D. (1990): *Mathematical programming methods in structural plasticity*, Springer Verlag, New York.

Lotfi, H.; Shing, P. (1994): Interface model applied to fracture of masonry structures, *J. Engng. Mech.*, ASCE, vol.120, pp.63-80.

Maier, G. (1970): Matrix structural theory of piecewise linear elastoplasticity with interacting yield planes. *Meccanica*, vol.5, pp.54-66.

Maier, G. (1976): Piecewise linearization of yield criteria in structural plasticity, *Solid Mech. Arch.*, no.2/3, pp.239-281.

Maier, G.; Carvelli, V.; Cocchetti, G. (2000): On direct methods for shakedown and limit analysis, Plenary Lecture, 4th Euromech Solid Mechanics Conference, Metz, June 26-30, *Eur J. Mech. A/Solids*, vol.19, Special Issue, pp.S79-S100.

Maier, G.; Comi, C. (2000): Energy properties of solution to quasi-brittle fracture mechanics problems with piecewise linear cohesive crack models. In: Benallal A. (ed.) *Continuous Damage and Fracture*, Elsevier, Amsterdam, pp. 197-205.

Maier, G.; Frangi, A. (1998): Symmetric boundary element method for discrete crack modelling of fracture processes. *Computer Assisted Mech. and Engng. Sciences*, vol.5, pp.201-226.

Mroz, Z.; Giambanco, G. (1996): An interface model for analysis of deformation behaviour of discontinuity. *Int. J. Num. Anal. Meth. Geomech.*, vol.20, pp.1-33.

Nappi, A.; Perego, U. (1988): Boundary element analysis by linearized nonlinear-elastic material models: an application to no-tension systems, *Engineering Structures*, vol.10, pp.146-156.

Tin-Loi, F. (1990): A yield surface linearization procedure in limit analysis. *Mech. Stru. & Mechines*, vol.18, pp.135-149.

Tin-Loi, F.; Ferris, M.C. (1997): Holonomic analysis of quasi-brittle fracture with nonlinear softening, In: Karihaloo B. L., Mai Y. W., Ripley M. I., Ritchie R. O. (eds.), *Advances in fracture research*. Pergamon, Oxford.

Xu, X.; Needleman, A. (1994): Numerical simulation of fast crack growth in brittle solids, *J. Mech. Phys. Solids*, vol.42, pp. 1397–1434.

Wei, Y.; Chow, C. L.; Liu, C. T. (2000): Damage analysis for mixed mode crack initiation, *CMES:Computer Modeling in Engineering & Sciences*, vol.1, no.4, pp.71-78.